Predictive Models for the Hydrothermal Liquefaction Products of Brown Macroalgae

Micheal Asama[1], Fernando Resende[1*], Aaditya Khanal[1*]

[1]The Jasper Department of Chemical Engineering, The University of Texas at Tyler

Corresponding author E-mail address: fresende@uttyler.edu; aadityakhanal@uttyler.edu

ABSTRACT

This study presents novel predictive models for HTL of brown macroalgae, describing the formation of biocrude, gas, biochar, and water-soluble compounds as products. The models account for the chemical composition of the macroalgae and explain the effects of time, temperature, pressure, and water-to-biomass ratio as input variables to estimate product yields from hydrothermal liquefaction (HTL). To achieve this goal, we used experimental kinetic data to develop a process simulation for batch HTL of macroalgae. We then applied the design of experiment (DOE) to generate simulation runs at different combinations of process variables. The results were used to develop predictive models describing the effects of such process conditions on product yields from HTL of macroalgae. Next, the predictive models generated were used to optimize the yield of bio-crude produced. Also, we used response surface methodology (RSM) to visualize the effect of process variables on product yields. Additionally, the models were validated against experimental data from literature, with 91% agreement within the 95% prediction interval for the biocrude yield model. Analysis of Variance (ANOVA) showed that the selection of operational parameters significantly affects biocrude yield. The optimal biocrude yield was 23% at 283°C, 200 bar, 54 minutes, and a water-to-biomass ratio of 10:1, with temperature and residence time as the significant variables that affect biocrude yield. Sensitivity analysis on the reaction rate constants allowed for the identification of significant paths that affect biocrude yield. The workflow presented in the study and the predictive models provide an accurate path for modeling various products from HTL of kelp.

Keywords: Hydrothermal Liquefaction (HTL); Kelp; Response Surface Methodology; Optimization, Biocrude Yield; Regression Model; Design of experiments (DOE)

1.0 INTRODUCTION

The concern over the environmental impact of fossil fuel emissions, the potential for its depletion, and price increases have driven significant research efforts toward sustainable alternatives for energy generation. Environmental sustainability, energy security, and global warming reduction have increased interest in alternative energy sources, which are closely evaluated as potential solutions to meet our energy needs more sustainably and responsibly [1,2]. Waste oils, agricultural and municipal waste, and specially grown inedible energy crops are among the second-generation feedstocks for biofuel that can substantially reduce the use of fossil fuels for transportation and chemicals[3].

Macroalgae, also known as seaweed, on the other hand, is an underutilized third-generation feedstock and commodity with significant commercial value and versatility, primarily for the production of food, cosmetics, and fertilizers[4]. Seaweed has several distinct advantages as a renewable energy source: first, it boasts high photosynthetic efficiency, allowing it to quickly produce large quantities of biomass[5]. Secondly, the feasibility of cultivation in various locations worldwide and the lack of competition for arable land and freshwater with food crops further enhance its potential as a renewable energy source. Finally, the potential for producing diverse value-added chemicals and biofuels makes kelp a particularly attractive resource. For these reasons, seaweed has become a topic of growing interest in Europe as a potential energy source, with an average yield of 15 to 20 dry tons per hectare per year[6,7]. Approximately 28 million metric tons of wet macroalgae biomass are produced annually via aquaculture, with an estimated value of over 7 billion dollars[8].

The conversion of seaweed into biofuels can be achieved via several processes. These processes can be broadly classified into biochemical, which include the fermentation of macroalgae to produce bioethanol[9], and thermochemical, such as pyrolysis[10], direct combustion[11], and the HTL of

macroalgae to produce bio-crude[1]. Biochemical conversion uses biological processes, such as fermentation or enzymatic reactions, to convert seaweed into fuels and other valuable chemicals. The efficiency of the biochemical conversion of seaweed to bioethanol is affected by several factors, including the type of seaweed, the choice of pretreatment, hydrolysis, and the fermentation method [7,12]. However, a significant hindrance to achieving high bioethanol yield is the need for microorganisms capable of effectively converting the diverse monomeric sugars[12]. On the other hand, thermochemical conversion, such as pyrolysis, gasification, combustion, and HTL, involves high temperatures and pressures to convert biomass into fuels and other value-added chemicals[13]. Due to its high moisture, alkali content, and low energy content, seaweed poses challenges for direct use in combustion, pyrolysis, or gasification processes. As a result, pretreatment is necessary to mitigate these issues and make seaweed a viable fuel source. HTL, on the other hand, employs water under high temperatures (200-350°C) and pressures (5–20 MPa) to transform the organic mass of seaweed into bio-crude, biochar, gas, and water-soluble compounds, thereby eliminating the need for initial drying of the macroalgae [14].

HTL uses water as a solvent and reactant to convert seaweed into useful products. Water has several valuable qualities when near its critical point. HTL of seaweed occurs in the subcritical region (liquefaction), where water is sustained in liquid form under pressure higher than the saturation pressure[15]. Hot compressed (subcritical) water is a suitable medium for effectively converting seaweed into four different phases (biocrude, water, gas, or solid char) of product due to its low viscosity and high solubility of organic compounds, among other properties[16–18]. In addition to its properties substantially different from water at ambient temperature, hot compressed water has a lower dielectric constant (e.g., 78 Fm^{-1} at 25 °C and 1 MPa to 14.07 Fm^{-1} at 350°C and 20 MPa [16,19]), which results in increased solubility of hydrophobic chemical molecules, such as free fatty acids [20,21].

The products from HTL of seaweed depend on the operating conditions and the chemical composition of the biomass[22]. During HTL, the lipid, protein, and carbohydrate fractions decompose into smaller

molecules in four phases: biocrude, water, gas, or solid char [23], as shown in **Figure 1**.

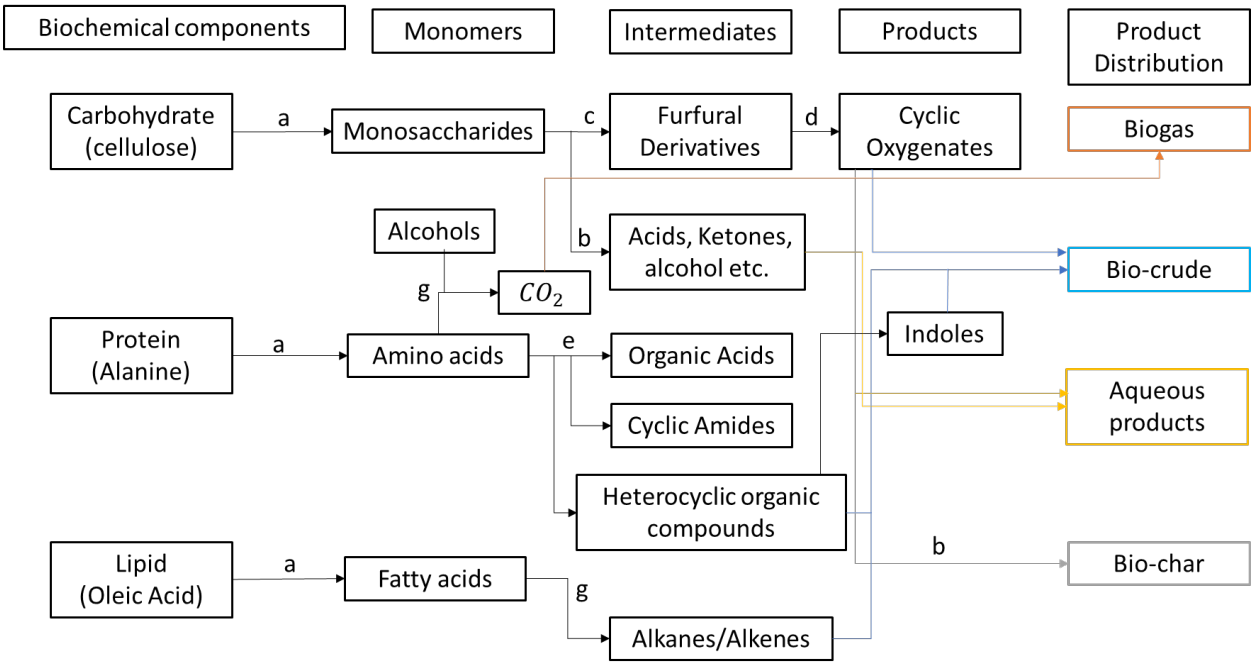

Figure 1. Possible Reaction Pathway for HTL of macroalgae biomolecules (a) Hydrolysis (b) Decomposition (c) Dehydration (d) Polymerization (e) Deamination (g) Decarboxylation[24]

Seaweeds generally contain a high fraction of carbohydrates. A study by Schiener et al. on four different species of macroalgae showed that the carbohydrates (cellulose, alginates, mannitol, and laminarin) fraction ranges from 63-79%[5]**.** A study by Galland-Irmouli et al. on the French Atlantic Coast macroalgae showed that the protein content, which includes a wide variety of amino acids (glutamic acid, aspartic acid, proline, glycine, alanine, valine, methionine, isoleucine, leucine, phenylalanine, lysine, and arginine) as building blocks, can range from 9 to 25%[25,29-32]. The biocrude produced from HTL of seaweed may contain significant amounts of nitrogen due to its high level of proteins[26]. In addition to carbohydrates and proteins, seaweed contains lipids, although less than what can be found in microalgae, with a maximum of 4.5% of its dry weight[27]. A variety of fatty acids makes up most of the lipid content in seaweed. The two fatty acids that were most commonly found in seaweed were palmitic and oleic acid[28].

The design and commercialization of an industrial-scale HTL process can be facilitated by the accessibility of predictive mathematical models that successfully describe the process[29] and provide reasonable estimates of the HTL products for a wide range of seaweed species and HTL operating conditions. Biller and Ross[13] used a combination of lipids, protein, and carbohydrates to develop a model for estimating biocrude yield from HTL of microalgae at 350℃ and 60 min. While the model provides good predictions for some microalgae, it is limited to one process condition (350℃ and 60 min) and only estimates the biocrude yield, not accounting for other products (aqueous product, biochar, and gas)[13,29,30]. To expand on the limitation of Biller and Ross's model, Valdez and Savage presented a kinetic model with a reaction network to describe the HTL of *Nannochloropsis sp*. This model provides a reasonable estimate of the four phases of products at different operating conditions. Initially, this model only applied to *Nannochloropsis sp* microalgae[29]. Later, this model was further expanded to a more general kinetic model for any microalgae species by including the biochemical composition (lipids, protein, and carbohydrate) of the microalgae species. While several models have been developed to estimate product yields from the HTL of microalgae, to best of our knowledge, two significant attempts have been reported for macroalgae. Raikova et al. proposed a biocrude additive model that predicts biocrude yield based solely on the lipid fraction of seaweed under a fixed set of process conditions[31]. However, this model does not account for the influence of key process parameters such as temperature, residence time, and pressure, limiting its applicability to broader HTL scenarios. Similarly, Bach et al. developed a linear model to estimate biocrude yield as a function of heating rates. However, this model is specific to a single seaweed species (*L. Saccharina*) and does not capture the influence of other process conditions or the yields of other product phases.

To date, no comprehensive models exist to predict the yields of all HTL product phases (biocrude, biochar, aqueous, and gas) across a range of process conditions. This study aims to address this gap. The models capture the combined influence of key process variables and the biochemical composition of brown seaweed, offering a more comprehensive approach to modeling HTL product distribution.

Therefore, in this work, we present novel predictive regression models to estimate the yield of HTL products (biocrude, biochar, gas, aqueous) for brown seaweeds. We used model compounds to represent the chemical composition of the seaweed species (*S. latissima*) and performed simulations at various process conditions (temperature, residence time, pressure, and water-to-biomass ratio). The carbohydrate fraction was represented by cellulose, protein by alanine, and lipid by oleic acid. The criteria for the selection of model compounds were: 1) the structural similarity to key chemical linkages found in the seaweed (*S. latissima*) biomass feedstock, 2) similarity to one of the various intermediate HTL products, and 3) the availability of kinetic data that accurately depicts the behavior of the compounds under HTL conditions. According to previous reports, using model compounds simplifies the process simulation and results in product yields similar to those from actual biomass [22,32–34].

The design of the simulation conditions followed the three-level central composite design. The results obtained from the simulations were used to create multivariate regression models to predict the yield of HTL products. This enabled us to understand the effects and interactions of the process variables on yields. We statistically analyzed our results using analysis of variance (ANOVA) to identify variables or combinations of variables contributing to the predictive model. Several researchers have used traditional experimental methods, such as one factor at a time (OFAAT), to explain the effect of temperature, residence time, pressure, and water-to-biomass ratio on product yield[1,3–5,26,35–38]. However, this method fails to capture the interaction effects of various factors on product yield. The present study utilizes response surface methodology to visualize this effect. Finally, the proposed model was optimized to obtain the operating conditions that maximize biocrude yield within the studied conditions range. The model was further extended to include various brown seaweeds that share a close range of chemical composition. The methodology used in this study can be applied to similar operations, and the results obtained show the significance of identifying the critical process parameters for optimizing the biocrude production from HTL of brown seaweed.

This article describes several components that contribute to the analysis of the HTL process with the goal of maximizing the biocrude yield: 1) the use of kinetic data from the literature to simulate the batch

HTL of seaweed; 2) the use of the design of experiments (DOE) in selecting conditions for the simulations; 3) the generation of predictive regression models to capture the effect of several operating parameters on product yields; 4) validation of the regression models; 5) the use of the regression models to maximize the biocrude yield; and 6) sensitivity analysis to identify essential reaction paths to increase biocrude production beyond the yields reported in this work.

2.0 METHODS

We developed a model to simulate a batch process for the HTL of *S. latissima* using SuperPro Designer v12. SuperPro Designer is a comprehensive and robust process simulation software developed by Intelligen, Inc. We simulated the liquefaction process using mixtures of model compounds based on the average chemical composition of *S. latissima,* which consists of 75% carbohydrate (cellulose), 18% protein (Alanine), and 7% lipid (oleic acid) on a dry ash-free basis (DAF)[28,39–41]. The DAF allows a focused evaluation of the reactive organic components of seaweed, which are primary contributors to products formed. Valdez and Savage (2014) proposed a bulk network of possible reaction pathways for the HTL of microalgae, as shown in **Figure 2**.

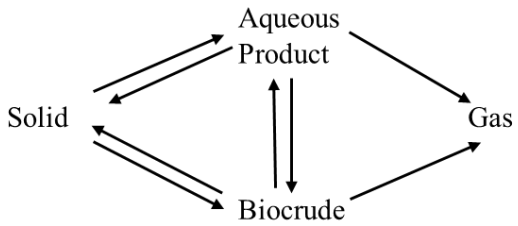

Figure 2. Possible reaction pathways for HTL of model compounds[29]

These pathways describe how HTL products are formed by considering the independent reaction of each model compound (cellulose, alanine, oleic acid) representing the chemical composition of seaweed[30]. The solid represents not only the initial biomass that undergoes the HTL process but also the biochar formed as a co-product of the process.

We used experimental kinetic data reported by Obeid et al. [33,34] for the HTL of each model compound. Therefore, no new experimental testing was performed in this work. The rate constants (k), pre-exponential factors (A), and activation energies ($\boldsymbol{E_a}$) are reported in **Table 1**. Kinetic data were fitted according to this pathway, as shown in **Figure 3**, and each rate constant is associated with the transition from one phase to another.

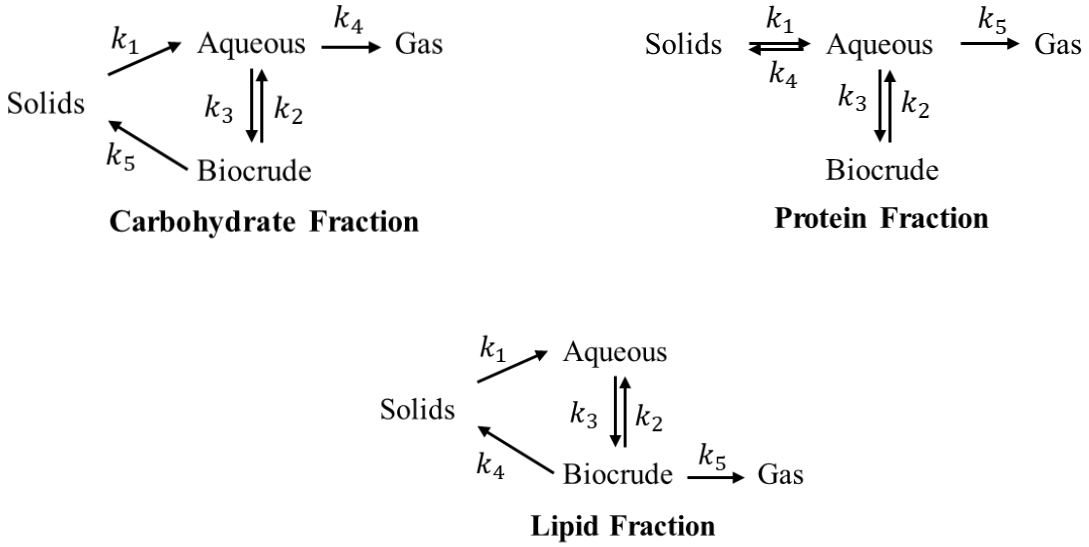

Figure 3. Reaction Pathways for Model Compounds adapted from [22,33,34]

Table 1. Kinetic Data for Model compounds adapted from [22,33,34]

Compound	Path	Reaction	k [°C](Sec^{-1})			LnA	E_a	Ref.
			Temperature (°C)				(KJ/mol)	
			250	300	350			

Carbohydrate	1	Solid to Aqueous	1.69	2.73	3.33	4.8±1.3	18.6±1.0	[33]
	2	Biocrude to Aqueous	3.19	3.97	8.35	7.0±3.4	25.6±2.8	[33]
	3	Aqueous to Biocrude	4.80	4.88	5.73	2.6±0.9	4.7±0.9	[33]
	4	Aqueous to Gas	1.20	1.29	1.40	1.1±0.1	4.2±0.1	[33]
	5	Biocrude to Solid	4.8	18.6	20.4	11.0±6.4	40.0±5.2	[33]
Protein	1	Solid to Aqueous	12.24	16.99	59.79	12.0±6.1	42.1±4.9	[22]
	2	Biocrude to Aqueous	7.87	59.24	51.48	12.8±11.4	45.4±9.2	[22]
	3	Aqueous to Biocrude	0.85	5.84	4.03	10.2±12.3	43.8±10.0	[22]
	4	Aqueous to solid	2.62	1.13	3.82	2.6±11.9	8.5±9.6	[22]
	5	Aqueous to Gas	0.36	0.38	0.38	-0.8±0.2	1.9±0.2	[22]
Lipids	1	Solid to Aqueous	33	45.13	60	7.2±0.1	16.1±0.1	[22]
	2	Biocrude to Aqueous	2.14	28.58	28.8	16.7±14.6	67.5±11.8	[22]
	3	Aqueous to Biocrude	12.89	48.19	60.00	11.9±6.0	40.1±4.9	[22]
	4	Biocrude to solid	3.23	3.23	3.30	0.6±18.5	0.1±15.0	[22]
	5	Biocrude to Gas	0.14	0.24	0.17	-0.3±4.4	6.7±3.6	[22]

A, E_a represent the pre-exponential factor and activation energy, respectively.

2.1 Process Flowsheet

The process flow diagram for HTL of model compounds representing brown seaweed (kelp) is shown in **Figure 4**. The macroalgae and water are combined in a mixer to form a slurry and then pumped to the HTL reactor. The reactor is heated to the target temperature (240–350°C) and pressure (120-200 bar) for the reaction, allowing a residence time of 5–60 minutes. The HTL process entails the conversion of biomass into four product phases, namely gas, biocrude, biochar, and aqueous phases.

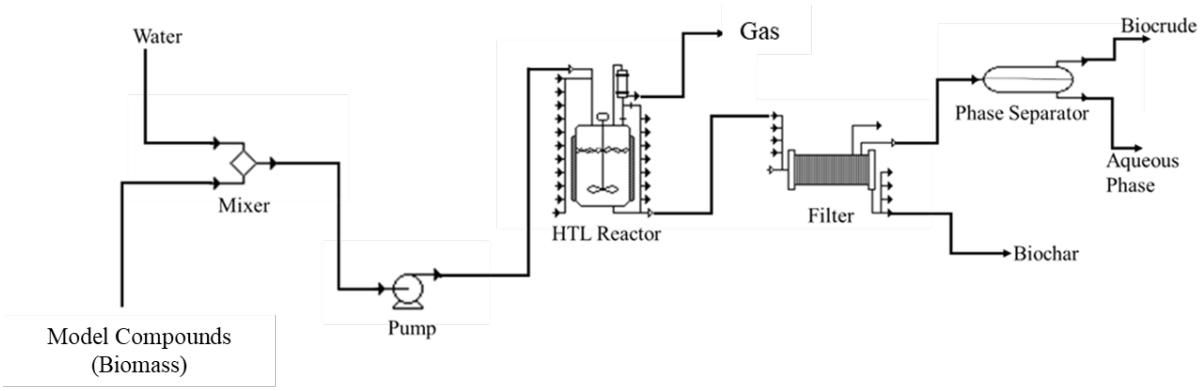

Figure 4. A batch system for HTL of model compounds representing brown seaweed (S. latissima)

Once the desired residence time in the reactor elapses, the reactor is cooled and depressurized to stop the HTL process and facilitate the removal of the gas from the resulting product. Subsequently, the remaining content is directed to a filter to separate the biochar component. In the subsequent stage, a cyclonic separator isolates the desired product, biocrude, from the aqueous phase, predominantly water and certain dissolved organic compounds. This separation step ensures the extraction and purification of the valuable biocrude component for further processing. The biocrude was modeled as a mixture of furfural, pyridine, and Octanoic acid obtained from the HTL of cellulose, alanine, and oleic acid, respectively. The gas produced from HTL of seaweed from experiment testing [37] majorly consists of CO_2. Hence, the gas in this work was modeled as CO_2. The solid biochar was modeled as ash to maintain the physical state as solid, while the aqueous product was obtained by difference method. This choice was based on results reported in prior studies[22,33,34]. All model compounds selected are predominant compounds in each product phase.

A prior study performed in our lab on the HTL of *S. latissima* [37] reported similar biocrude composition as results reported for the model compounds used in this study [22].

The HTL product yields were calculated using **equation (1-3)** below.

$$Biocrude\ Yield(wt\%) = \frac{mass\ of\ biocrude}{mass\ of\ the\ dried\ kelp}\ \text{x}\ 100 \quad (1)$$

$$Biocrude\ Yield(wt\%) = \frac{mass\ of\ biocrude}{mass\ of\ the\ dried\ kelp}\ \text{x}\ 100 \quad (2)$$

$$Biochar\ Yield(wt\%) = \frac{mass\ of solid\ char}{mass\ of\ dried\ kelp}\ x100 \quad (3)$$

2.2 Design of Simulation Runs

We used the design of experiments (DOE) to select process variables and determine their effects on the product yields (biocrude, aqueous, biochar, and gas yield). DOE employs statistical techniques to assess data and forecast product composition within the limits chosen for the simulation run design [42]. The simulation runs in this work were created using the response surface's central composite design (CCD), which involved different levels of the residence time, temperature, water-to-biomass ratio, and pressure, recording the impact of these inputs on the product yields, as shown in **Table 2**. The CCD consists of a two-level factorial design with an additional 2k for the axial points, where k is the number of independent variables and center points that provide information about the pure error or variability in the system [42].

Table 2. Simulation Run Design

Levels	**-1**	**0**	**1**
Temperature (T, °C)	240	320	400
Residence Time (Ti, minutes)	5	32.5	60
Water-to-biomass ratio (WB, g/g)	1	5.5	10
Pressure (P, bar)	120	160	200

We conducted the DOE with MATLAB, resulting in 30 runs. The design was implemented using custom scripts to systematically vary the levels of the independent variables (residence time, temperature, water-to-biomass ratio, and pressure) and record the corresponding response variables (biocrude, aqueous, biochar, and gas yield).

3.0 RESULTS AND DISCUSSION

3.1 Hydrothermal Liquefaction

Figures 5(a) and 5(b) shows the results obtained at a single experimental condition. The HTL of each model compound resulted in the decomposition of the solid phase via hydrolysis at 320℃, 160 bar, and a water-to-biomass ratio of 10:1. Each model compound is rapidly converted to simpler molecules, as shown in **Figure 5(a)**. The initial conversion stage involves hydrolysis of cellulose, alanine, and oleic acid, forming an aqueous phase. Compounds in this phase then undergo further reactions to produce biocrude, gas, biochar, and aqueous products. The downward trend in concentrations of the starting model compounds confirms the expected progression of the first conversion stage. As shown in **Figure 5(b)**, the concentration of biocrude from cellulose is the highest due to the high carbohydrate concentration of the seaweed. Following this is the concentration of biocrude from alanine and then oleic acid.

Figure 5c shows the effect of temperature, with collected simulation data for the yields of the four phases of the products at varying temperatures (250℃-400℃) at a constant residence time (60 minutes) and water-to-biomass ratio (10:1). The results show that the biocrude yield increases slightly with temperature to a maximum of 21% at 300℃. Further increase in the temperature increased the yields of gas and solid residue. As the temperature increased above the critical temperature of the water at 374℃, the biocrude yield dropped. A high yield of aqueous product was formed at lower temperatures and decreased as temperature increased, while the gas and biochar yields increased with temperature.

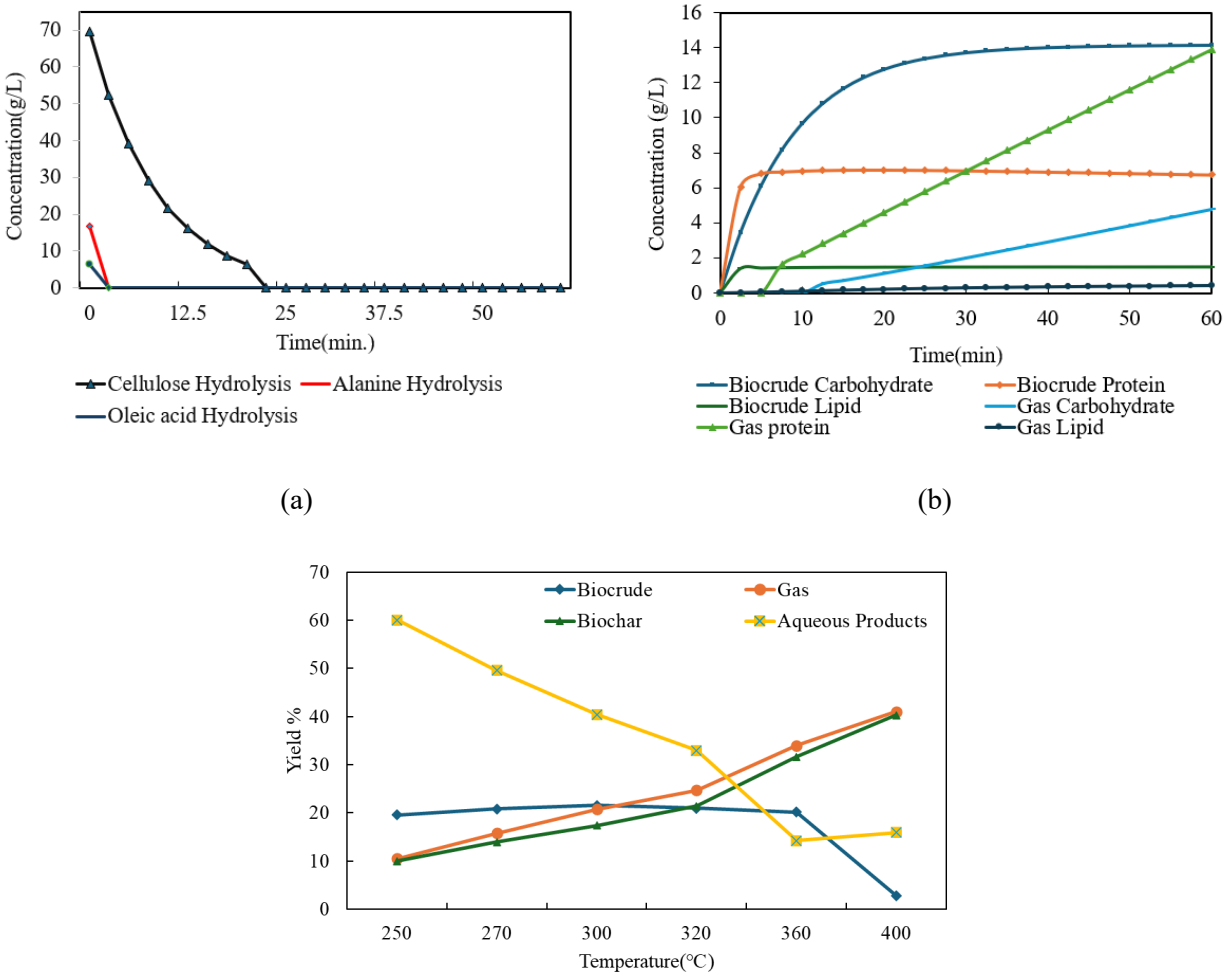

Figure 5. Plots from the simulation using kinetic data: (a) The conversion rate for each model compound, and (b) the concentration-time plot for biocrude and gas. (c) effect of temperature on yield of products from HTL of S. Latissima using simulation data at constant residence time(60minutes), pressure (200bar), and water-to-biomass ratio 10:1

3.2 Regression Model Fitting

The results obtained from the simulation for HTL of seaweed at various levels of independent variables using CCD are presented in the supplementary material (supplementary table S1). The data was used to develop regression models to capture the effect of temperature, pressure, residence time, and

water-to-biomass ratio on product yields from the HTL of the brown seaweed (*S. latissima*). The general form of product yields is shown in **equation 4,** and coefficients of model terms are represented as alphabets (*a*-*i*) are presented in **Table 3**.

$$Yields(\%) = a + b(T) + c(P) + d(WB) + e(t) + f(T * WB) + g(T * P) + h(T * t) \quad (4)$$
$$+ i(WB * t) + j(T^2) + k(t^2) + l(T^2 WB)$$

Where *T*, *t*, *P*, and *WB* represent temperature, residence time, pressure, and water-to-biomass ratio, respectively

Table 3. Table of coefficients for model terms

Coefficients	Biocrude	Gas	Aqueous Product	Biochar
a	-90.81	+168.90	-191.58	+424.86
b	+0.57	-1.39	+1.74	-2.58
c	+0.0065	+0.46	+0.13	+0.0000021
d	+4.73	-5.55	-1.81	-42.96
e	+0.18	-0.53	+2.11	-3.086
f	-0.0099	+0.026	0	+0.31
g	0	-0.0019	0	0
h	0	0	0	+0.0053
i	0	0	-0.070	0
j	-0.00090	+0.0030	-0.0033	+0.0042
k	-0.0020	+0.0097	-0.024	0.016
l	0	0	0	-0.00054

The regression model's ability to predict the biocrude yield within the range of conditions studied was revealed by the coefficient of determination $R^2 = 0.96$ and adjusted $R^2 = 0.94$, which measures the percentage (96%) of the response variable's overall fluctuation accounted for by the model. The closer the R-squared value to 1, the better the model fits the data, so a value of 0.96 suggests a solid relationship

between the independent and the dependent variables. The adjusted R-squared value measures the model's performance by accounting for only those independent variables that significantly explain the variability in the dependent variable. The predictive model for gas yield has a $R^2 = 0.96$ and adjusted $R^2 = 0.94$ while the predictive model for the aqueous product has a $R^2 = 0.91$ and adjusted $R^2 = 0.88$. The predictive model for biochar has a $R^2 = 0.76$ and adjusted $R^2 = 0.64$. The relatively low R^2 and adjusted R^2 observed for biochar can be attributed to the model's inability to account for the repolymerization of intermediates interactions during HTL, which are known to contribute significantly to biochar formation.

Next, we conducted ANOVA examinations to determine the statistical significance of the suggested model terms. This test, employed in statistical analysis, evaluates the importance of each model term and its collective impact on the response based on the p-value.

The results of the ANOVA analysis for the models can be found in the supplementary material (supplementary table S2-S5). Terms with p-values lower than 0.05 are considered statistically significant. In contrast, terms with p-values greater than 0.05 are excluded from the model because they do not significantly affect the model response.

The F-value, commonly referred to as the F-statistic is a metric used to compare the variability between group means relative to the variability within groups. The regression models generated in this work are statistically significant, as shown by their F-values of 167.15, 53.77, 29.74, and 5.7 for biocrude, gas, aqueous, and biochar models, respectively. A high F-value for the model provides strong evidence against the null hypothesis that all regression coefficients are zero. It also implies that at least one or more independent variables (*T, t, P, WB*) in the model contribute significantly to explaining the variability in the response variable (biocrude, gas, aqueous, and biochar yield).

3.3 Model Validation

The predictive regression model developed for the yield of products from the HTL of brown seaweed (*S. latissima*) was first validated by examining its predictive performance. We compared the predicted yields generated by the regression model against the corresponding actual (kinetic model)

values from the simulation shown in **Figure 6**. Next, we compared experiment yields from several literature reports on HTL of brown seaweed with the predicted yields from the regression models at similar conditions. These experimental values provided a standard against which we could assess the accuracy of our predictions since they reflected actual outcomes of the HTL process (**Figure 7)**. The predictive regression model is applicable for brown seaweeds, as it was developed using their specific chemical composition (lipid, carbohydrate, and protein content). Applying it to other seaweed types with different chemical profiles may reduce its accuracy.

3.3.1 Validation with Kinetic Model

As shown in **Figure 6**, the yields from the predictive models (predicted yield) based on the selected variables were plotted against the actual kinetic yields (actual yield) from the simulation in a parity plot. The diagonal 45-degree line on the plot represents a perfect agreement between the predictive and kinetic models. The statistical analysis shows that the simulated runs fit the selected regression model in **equation 4** well, with a mean standard deviation of residuals of 1.018, 1.015, 1.101, and 2.181 for biocrude, gas, aqueous, and biochar products, respectively. This suggests that the predictive regression models appropriately depict the correlation between the studied variable and correctly capture the underlying system, with few discrepancies. The mean standard deviation of residuals measures the error between the predictive model and the actual kinetic model yield, indicating the predictive model's accuracy in predicting the actual yield of products from HTL of seaweed.

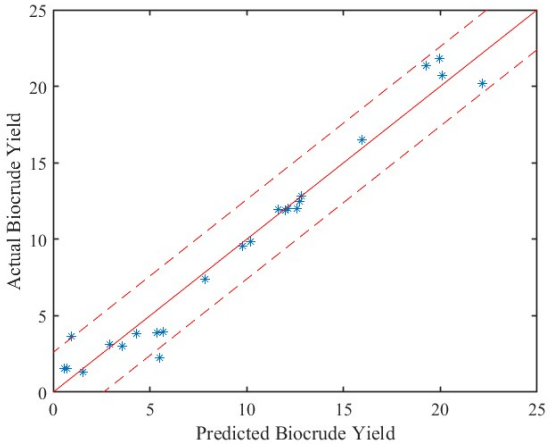

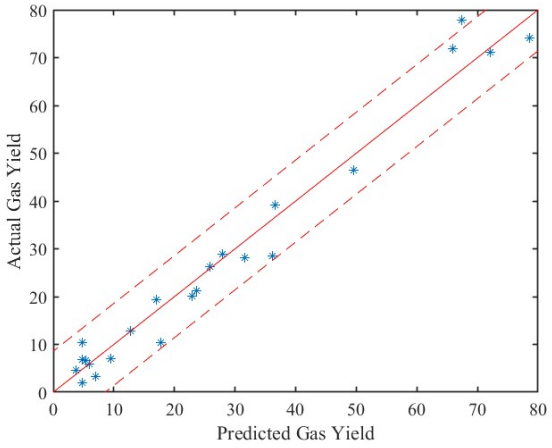

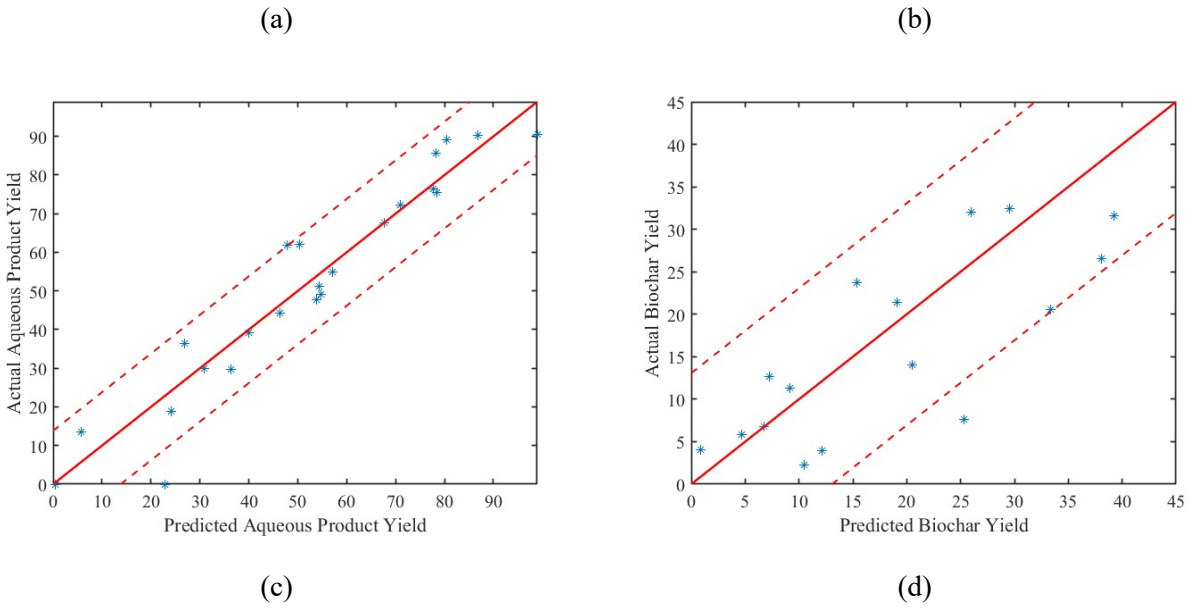

Figure 6. Parity plot for yield of (a) Biocrude (b) Gas (c) Aqueous Product and (d) Biochar. The actual yield represents the product yield from the kinetic model, while the predicted yield represents the product yield from the predictive model

3.3.2 Validation with Experimental Results

The predictive models were developed using model compounds to represent the chemical composition associated with one specific species of seaweed (*S. latissima*). Here, we validate our models with experimental yields for HTL of several species of brown seaweed, which typically have high carbohydrate and low lipid content. The table showing experimental conditions and HTL product yields can be found in the supplementary material (supplementary table S6) provided in this report.

Figures 7(a) and 7(b) show that the biocrude and gas predictive models performed well by predicting yields close to the experimental yield with a residual error between ±3.2 at the same experimental conditions. The model performed well for species like *S. Latissima*, *Laminaria saccharina, Ascophyllum nodosum, Sargassum tenerrimum,* and *Fucus ceranoides***.** The mean residual error measures the mean error between the predicted and experimental yield and was found to be 2.82., The standard deviation of residuals, which measures how dispersed the data points are from the mean of residuals, was 5.47.

It is essential to highlight that despite good agreement between the model predictions and experimental data, some deviations still result from intrinsic errors in experimental procedures, variations in feedstock properties, or other external factors.

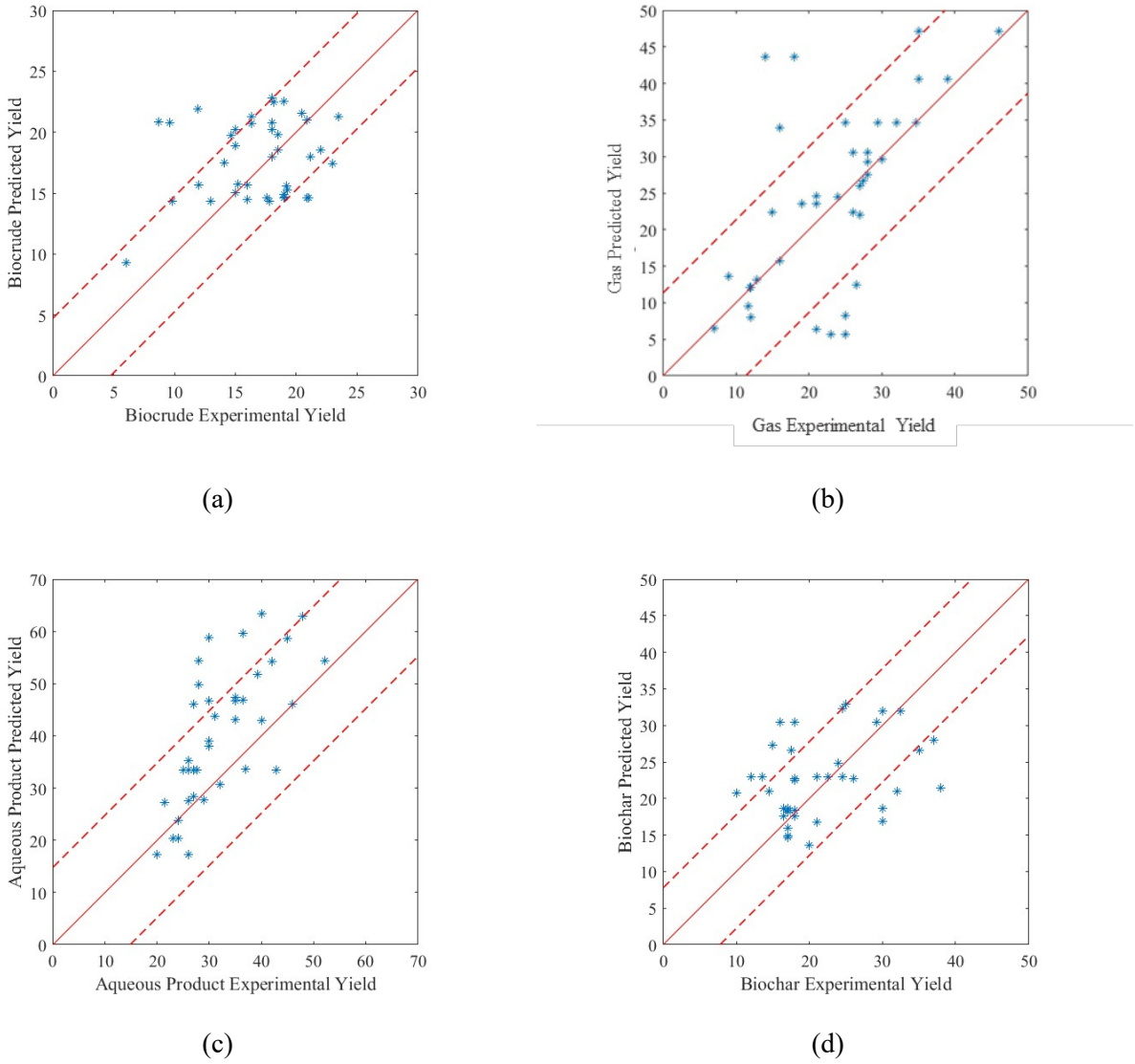

Figure 7. Predicted vs. experimental yields:(a) Biocrude, (b) Gas, (c) Aqueous, (d) Biochar with 95% predictive interval. This plot compares HTL product yields from the predictive model and experimental HTL product yields

One of these factors is the Maillard reactions, which are synergistic interactions between protein and carbohydrate intermediates. This is one among multiple chemical reactions involved in the hydrothermal

conversion and may increase the yield of biocrude by up to 25% more than the individual, independent reactions of each of the model compounds[43]. In this study, the HTL process is modeled as a set of independent reactions without interactions between intermediates of the resulting products. This approximation may lead to variations between the predicted and experimental yields.

We have accounted for these variations using the 95% predictive interval. The 95% predictive interval is a statistical measure that provides a range where the experimental yield will fall 95% of the time, based on the mean predicted yield and standard error of prediction. As shown in **Figure 7(a),** 92% of the experimental data used in validating our models falls within the 95% prediction interval. While 90% of the data falls within the 95% predictive interval in **Figure 7(b)**. The model's strength is supported by the large percentage of data points within the predictive interval. The experimental data outside the 95% predictive interval may result from the factors we did not account for, like the reactions between intermediate products during the HTL process and significant variation between the composition of the seaweed species and the one used for our simulation. Future studies will aim to capture these interaction effects and variations in the chemical composition of these macroalgae by considering other advanced statistical and machine-learning models to capture variations in the chemical composition.

Figures 7(c) and **(d)** show the experimental versus predicted yield for aqueous and biochar products. The aqueous product model effectively predicted the experimental yields from the literature. Results showed that the model accounted for 84% of the data set within the 95% predictive interval. The predictive model for the biochar product was less capable of predicting the experimental yield of biochar from the literature. The model over-predicts the experimental yield at lower temperatures between 240-300℃ and under-predict as well above 300℃ (reported experimental yields provided in the supplementary material table S6).

The regression model predicted 65% of the experimental data within the 95% confidence interval. The inability of the models to capture interactions between intermediates during HTL reaction leads to a deficiency that is more pronounced for the biochar and aqueous phase.

3.4 Response Surface Analysis

Once the model is validated, the response surface analysis enables one to evaluate and visualize the effect of combining multiple variables on product yields.

3.4.1 Effect of Temperature and Residence Time on HTL Product Yields

The effect of temperature and residence time on yields at a constant pressure of 200 bar and water-to-biomass ratio of 10:1 on HTL can be approximated by a parabolic curve, as shown in **Figure 8**. The yield of biocrude was observed to increase with temperature up to a maximum of about 23% between 260℃-300℃. As temperature increases beyond this range, the HTL process favors gas production, reducing biocrude yield. This result suggests a temperature range in which the biocrude yield is maximized (260-300℃). The decrease in biocrude yield as the temperature rises toward the gasification temperature suggests further thermal decomposition into smaller molecules at higher temperatures.

Overall, a long residence time (30-60 minutes) favors the formation of biocrude at low temperatures (between 240-330℃), while a short residence time below 30 minutes is preferred for high temperatures (above 340℃). Prolonged residence time at high temperatures causes the degradation of the biocrude, leading to an increase in biochar and gas formation. At lower temperatures, the macromolecules in the macroalgae undergo hydrolysis to form smaller molecules, followed by reactions like dehydration, decarboxylation, and deoxygenation. At very high temperatures, the rate of re-polymerization increases, leading to an increase in biochar formation while the rate of hydrolysis is reduced [36].

Some researchers have reported similar observations. Anastasakis and Ross observed for the HTL of *L. saccharina*, that the biocrude yield reaches a maximum of 19.3% at a temperature of 350℃, with a residence time of 15 min[1]. Qu et al. (2003) carried out HTL of *L. Cunninghamia* and reported a maximum yield of 17% for biocrude at 340℃, 30 minutes, and observed a reduction of biocrude away from this temperature range[36]. They suggested that this effect is caused by the competition between hydrolysis and re-polymerization reactions during HTL. The initial reaction stage involves biomass decomposition and depolymerization into smaller compounds. At temperatures above 340℃, the

compounds tend to undergo re-polymerization, reducing the biocrude yield. Zhou et al. (2010) found that 300℃ and 30 minutes are enough to produce the maximum biocrude of 23% from *E. prolifera.* A deviation from this condition reduces the biocrude yield[35]. Yin et al. also observed a peak at 310℃ with a biocrude yield of 34% and a decrease in biocrude yield as temperature increases.

The residence time has a similar effect on the biocrude yield, though not as pronounced as the effect of temperature, as shown in **Figure 8(a)**. The biocrude yield increases with residence time for about 40 minutes at moderate temperatures (250-320℃), after which the yield reaches a plateau. Longer residence times at temperatures above 350℃ tend to reduce biocrude yield. Overall, temperature and residence time strongly affect the yields of biocrude and its co-products from HTL. According to a literature report, a moderate temperature (300-320 ℃) and sufficient residence time (30-60 minutes) promote the formation of high molecular weight, viscous and dense biocrude[44].

High temperature and long residence times favor high gas yield from the HTL process, significantly beyond 330℃, as shown in **Figure 8(b).**

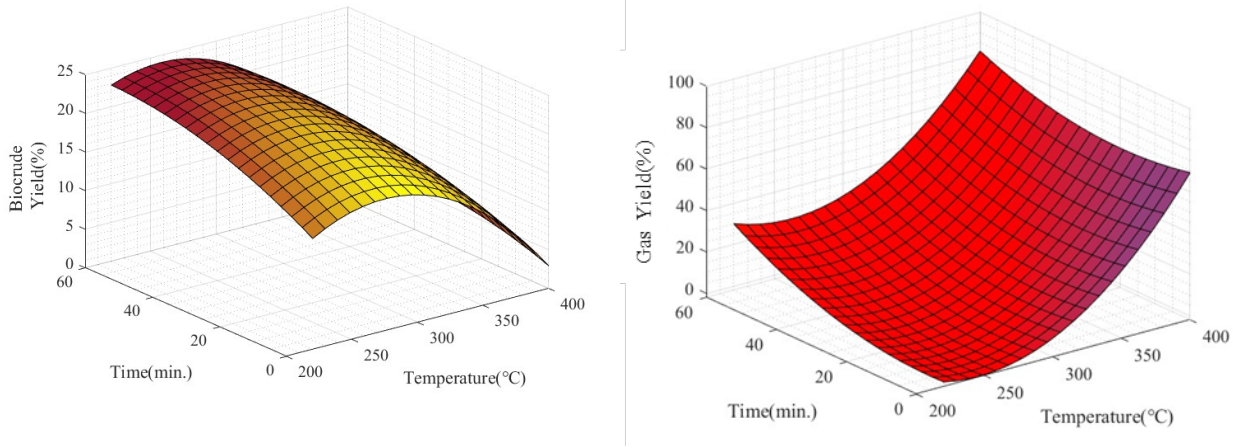

(a) (b)

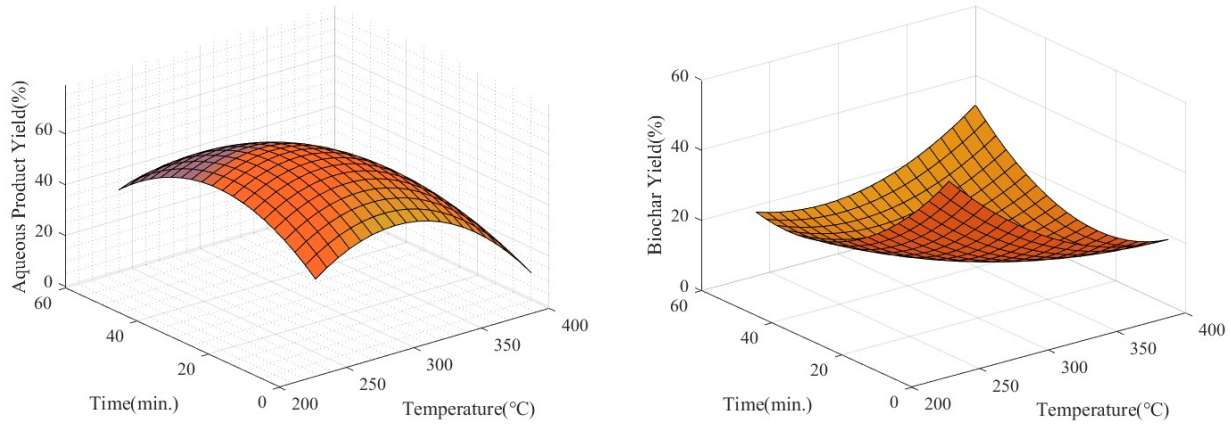

(c) (d)

Figure 8. Response surface plot obtained from the predictive model showing the effect of residence time and temperature on(a)biocrude, (b)gas, (c)aqueous, and (d)biochar at 200 bar and water-to-biomass ratio 10:1

The effect of temperature and residence time on aqueous products is depicted in **Figure 8(c).** As temperature increases, the yield of aqueous products increases to a maximum of about 40% at a temperature between 300-320℃, reducing as the temperature increases further away from this range. We hypothesize that temperatures within the range of 300-320℃ tend to promote hydrolysis and depolymerization of the biomass, leading to a high yield of aqueous product.

Figure 8(d) depicts the effect of temperature and residence time on biochar yield from the HTL of macroalgae. Low temperatures between 240-330℃ lead to a low yield of solid residue at residence time above 30 minutes, while operating at high temperatures causes cracking of the biocrude molecules, causing re-polymerization to promote biochar formation.

Long residence times lead to biochar formation as temperature increases towards the gasification temperature. Velasco Calderón et al. described biochar as a carbonaceous product called humins, formed during acid-base condensed phase conversion of biomass intermediates[45]. Jatoi et al., while studying the effect of residence time on biocrude yield, observed that the kinetics of HTL strongly affected the residence time and that a maximum yield of biocrude can be achieved with sufficient residence time,

while excessive long times lower the biocrude yield, leading to the formation of biochar and gaseous products[46].

3.4.2 Effect of Pressure and Water-to-Biomass Ratio on HTL Yields

In this section, we varied the pressure and water-to-biomass ratio to verify their effects on product yields at 320℃ and 60 minutes. Pressure and temperature must be adjusted to ensure water remains liquid, maintains high density, and is effective as a solvent. As shown in **Figure 9(a),** as pressure increases in the range of 120-200 bar, it promotes the production of biocrude between 20-22% with a water-to-biomass ratio of 10:1. The effect of pressure on biocrude yield is not as significant as the effect of temperature and residence time. Pressure shows a slightly linear relationship with biocrude yield; we believe that pressure levels above 113 bar (saturation pressure of water at 320℃) are sufficient to maximize the biocrude yield. ANOVA analysis in the supplementary material (supplementary table S2-S5) shows p-values greater than 0.05 for pressure in all models except the biogas yield model, indicating its minimal effect on product yields.

Since water serves as a hydrogen donor and a solvent for hydrolyzing the high molecular weight carbohydrates in biomass, the water loading in the system is a crucial parameter [47]. As shown in **Figure 9(a)**, the biocrude yield increased linearly with the water-to-biomass ratio, with the maximum biocrude yield of about 21% at water-to-biomass of 10:1. A similar result was reported by Anastasakis et al., during the HTL of *L. Saccharina*: the maximum biocrude yield was obtained when 3g of the seaweed reacted with 30 mg of water, and any further increase in the amount of water did not significantly increase the biocrude yield. An increase in the water-to-biomass ratio increases the yield of these products. Pressure has a minimal effect on both gas and aqueous products. At a water-to-biomass ratio of 10:1, an increase in pressure decreases the yield of gas, as shown in **Figure 9(b),** while it increases the yield of aqueous product, as shown in **Figure 9(c).**

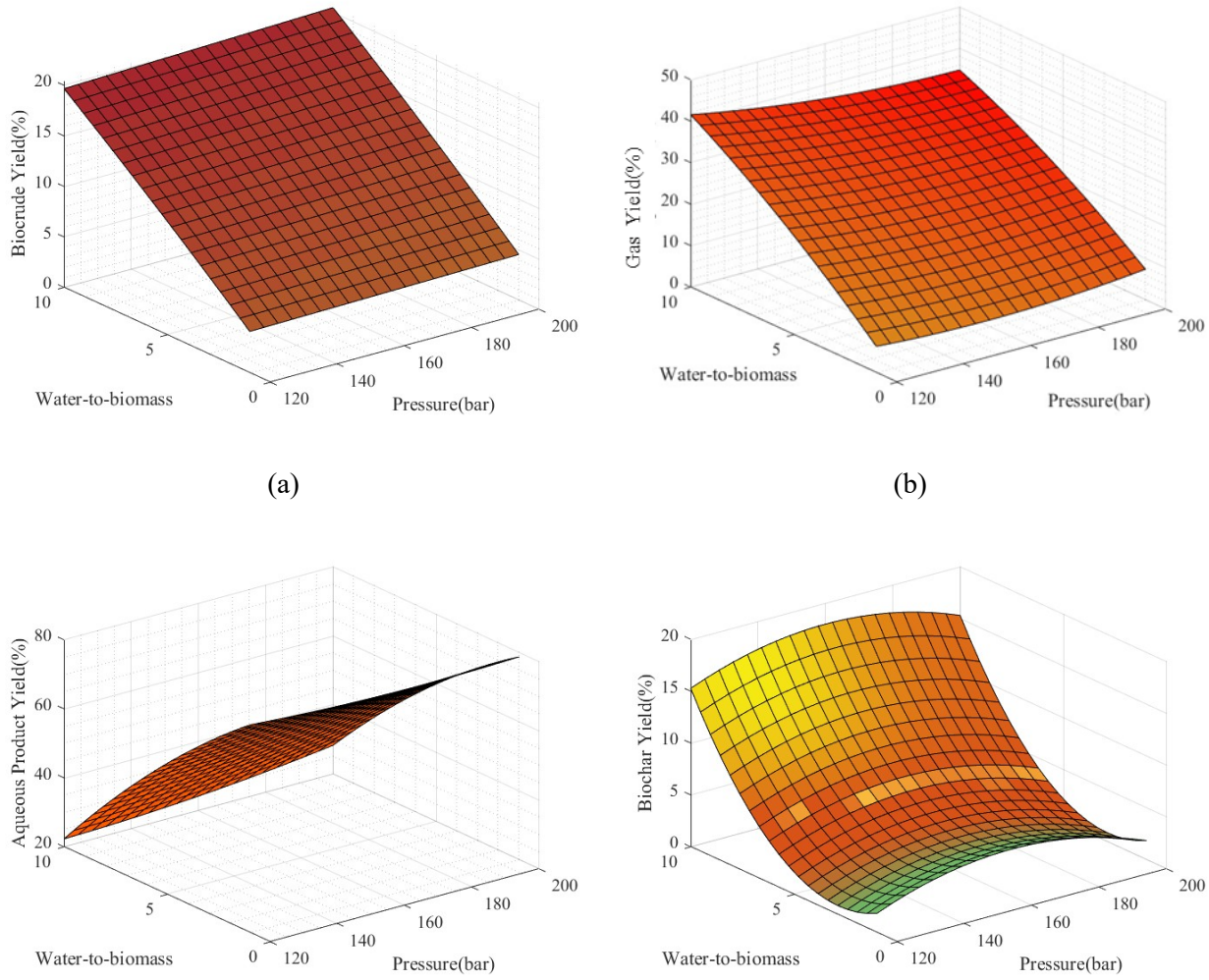

(a) (b)

(c) (d)

Figure 9. Response surface plot obtained from the predictive model showing the effect of water-to-biomass and pressure on (a) biocrude, (b) gas, (c) aqueous, and (d) biochar at 320℃ and 60 minutes residence time.

3.5 Optimization of Selected Factors to Enhance Biocrude Yield

Section 3.4 reported the investigation of factors that contribute to the production of biocrude. In HTL, one is usually interested in maximizing the yield of biocrude as an alternative fuel. Here, the results from the previous section lead to the identification of optimal conditions to maximize biocrude yield. We used the simplex search method of Lagaris[48] on MATLAB to iteratively optimize the model by maximizing the biocrude yield predictive model in **equation (4)** as the objective function and locating the

optimum biocrude yield, as shown in **Figure 10**. Similar to linear programming, this approach begins with an initial viable solution, which is typically an estimated point in the feasible region, then iteratively traverses a set of points that together constitute a simplex. The algorithm converges to a local optimum of the objective function by modifying the simplex's shape and location after evaluating the objective function at each iteration's vertices.

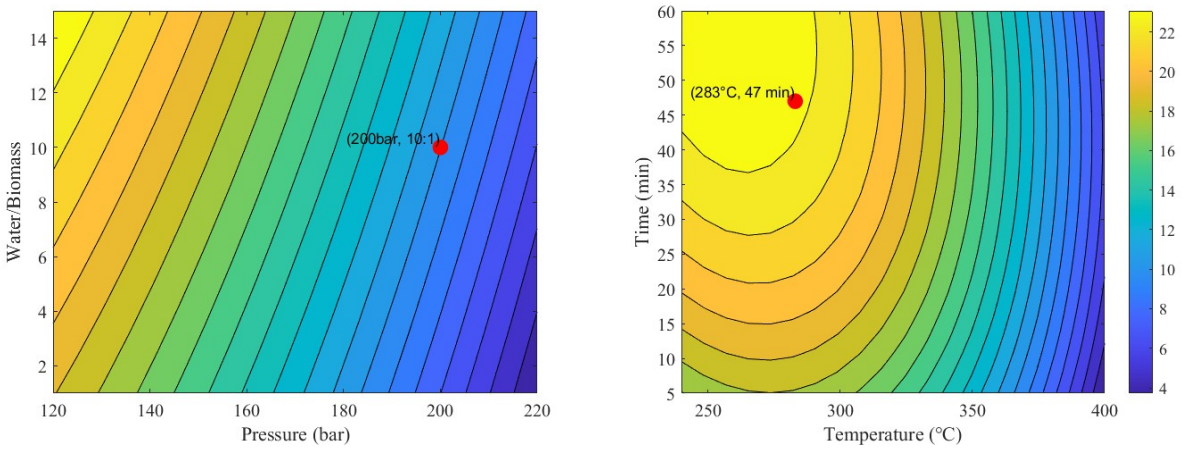

(a) (b)

Figure 10. Numerical Optimization of the predictive model for optimum biocrude yield.

The optimal biocrude yield was found to be 23% for temperature, pressure, residence time, and the water-to-biomass ratio of 283°C, 200 bar, 47 minutes, and 10:1, respectively. This combination of variables maximizes the yield of biocrude from HTL within the entire range of parameters studied.

3.6 Sensitivity Analysis

In this section, we are interested in determining how much single reactive steps from the kinetic model affect the biocrude yield. Reaction pathways shown in **Figures 2 and 3** include the breakdown of macromolecules into biocrude, the biocrude to aqueous product, biocrude to gas, the aqueous product to gas transformation, and the subsequent reactions that either promote or inhibit the formation of biocrude.

Identifying which reaction pathways that are most sensitive to changes in process conditions is essential for maximizing the biocrude yield while minimizing undesirable by-products like biochar or gas.

The sensitivity analysis is a valuable tool for examining and identifying critical reaction paths that significantly affect biocrude yield. This approach quantifies the impact of varying rate constants for individual reactions on the overall product yield, allowing us to pinpoint the most critical reactions that influence biocrude yield

The sensitivity coefficient $S_{i,j}$ can be calculated using the equation:

$$S_{i,j} = \frac{\partial lnC_i}{\partial lnk_j} = \frac{\frac{\Delta C_i}{C_i}}{\frac{\Delta k_j}{k_j}} \quad (5)$$

In **equation (5)**, i represents HTL products, j represents one of the reactions in the pathway, C_i, $\Delta C_i, k_j, \Delta k_j$ represents concentration, change in concentration of products, rate constant, and change in rate constant. To calculate the sensitivity coefficients, we applied a positive 5% variation to each rate constant and then rerun the kinetic model to compute the change in concentration (ΔC_i) for each HTL product.

The previous discussion showed a maximum biocrude yield of 23% can be obtained at 283℃, 200 bar, 54 minutes, and a 10:1 water-to-biomass ratio. For this reason, we computed the sensitivity coefficient around these conditions, and the results are presented in **Figures 11** for carbohydrates, proteins, and lipids.

The sensitivity analysis under optimal conditions revealed that the aqueous-to-biocrude reaction with rate constant k_3 has the most significant influence on the biocrude yield from the carbohydrate fraction of the macroalgae, as shown in **Figure 11(a)**. To maximize biocrude yield, it is essential to adjust process variables such as reaction temperature, pressure, and residence time to conditions that favor the aqueous to biocrude conversion. For instance, increasing the temperature to its optimal value can accelerate the

conversion of intermediate products in the aqueous phase to biocrude, while maintaining optimal pressure ensures that the aqueous phase remains at a density conducive to biocrude formation. The analysis also showed that biocrude production is minimally affected by the biocrude-to-aqueous phase reaction with rate constant k_2, exhibiting no significant impact on any product phases. This suggests that the rate constant k_2 is inconsequential to the overall process, and the products in the aqueous phase likely originate directly from the hydrolysis of carbohydrates rather than the degradation of biocrude. In contrast, the analysis shows that gas formation is sensitive to the aqueous-to-gas reaction, highlighting this pathway as a critical driver in producing gaseous products. Biochar formation, on the other hand, is primarily governed by the aqueous phase-to-biocrude reaction and the subsequent biocrude-to-biochar conversion. These pathways significantly contribute to the accumulation of solid residues during the HTL process. The formation of humins, as described by Jatoi et al., is linked to the degradation of biocrude, further emphasizing the role of these reactions in char production[46].

Figure 11(b) shows that, at optimal conditions, the hydrolysis of the protein to form monomers with a rate constant k_1 is not a significant reaction, as none of the four products depend on this reaction. However, the biocrude yield from the protein fraction strongly depends on the aqueous to biocrude and biocrude to aqueous reactions. Therefore, to maximize biocrude production from the protein fraction of the seaweed, it is essential to adjust reaction conditions and use catalysis that maximizes the conversion of aqueous phase products to biocrude. Additionally, the formation of biochar and biogas are sensitive to the aqueous-to-biochar and aqueous-to-biogas reactions.

The formation of the HTL products does not depend on the reaction that converts the lipid fraction to the aqueous phase, as shown in **Figure 11(c)**. The lack of sensitivity indicates that the hydrolysis of the lipid fraction does not directly contribute to biocrude formation via the aqueous conversion pathway. Instead, biocrude, gas, and biochar production are more sensitive to the reactions that convert aqueous into biocrude and biocrude into aqueous-phase products. This suggest that biocrude formation from the lipid fraction relies on reactions that convert intermediates in the aqueous phase into

biocrude. Therefore, to maximize biocrude yield from the lipid fraction of the biomass, the conditions must favor the aqueous to biocrude reaction, or a catalyst must be used to promote this reaction.

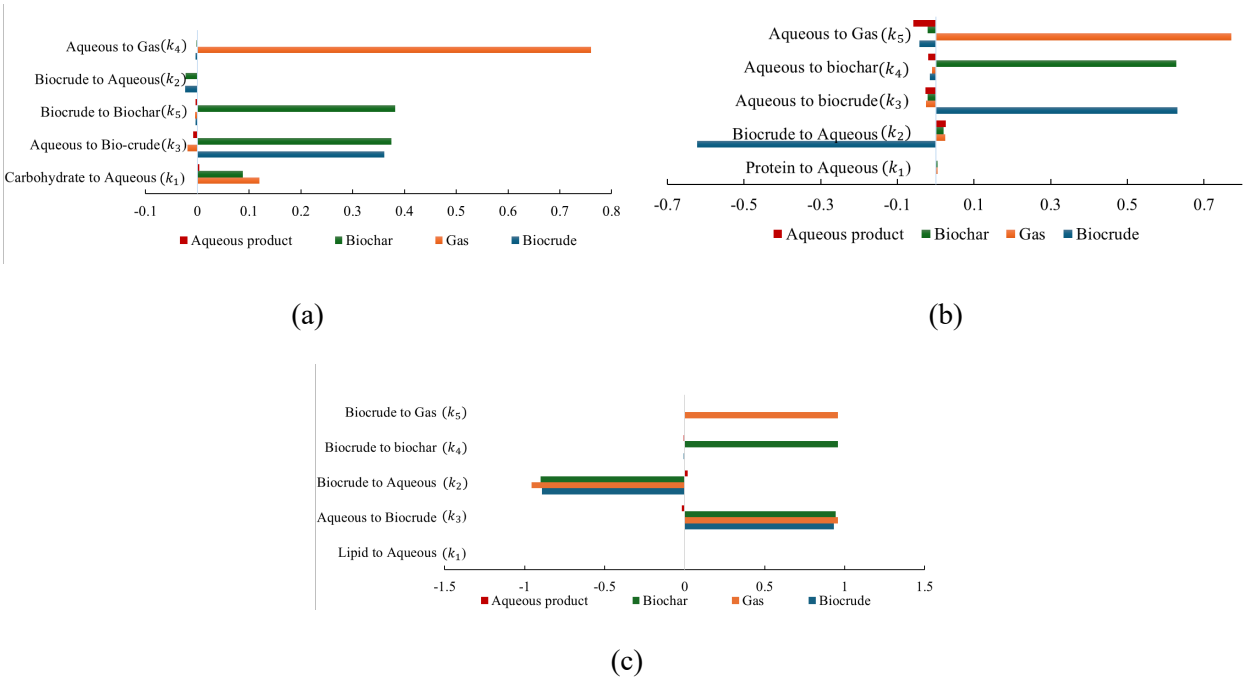

Figure 11. Sensitivity analysis on reaction kinetic paths from Figure 3 (a) Carbohydrate (b) Protein (c) Lipid Fraction

Overall, the aqueous-to-biocrude reaction plays a pivotal role in biocrude production from HTL of all seaweed fractions, indicating that water-soluble compounds are a significant precursor for biocrude formation. To optimize this conversion, various studies have highlighted the importance of catalytic interventions[49–53]. Specifically, heterogeneous catalysts, such as Pt/C, Ru/C, and Pt/C + Ru/C, have been shown to enhance biocrude yields by reducing the loss of the water-soluble organic to the aqueous phase[49]. These catalysts promote essential reactions like hydrogenation and decarboxylation, thereby facilitating the conversion of aqueous-phase organics into biocrude.

4.0 SUMMARY AND CONCLUSIONS

This study provides new insights into the effect of operating conditions on seaweed product yields during HTL. The regression models developed from kinetic data successfully captured the behavior of the four product phases (biocrude, gas, biochar, and aqueous phase) under varying HTL conditions. Our findings reveal that temperature and residence time are the primary factors affecting biocrude yield, with an optimal range identified at moderate temperatures (250-320°C) and residence times of around 40 minutes. Beyond these conditions, higher temperatures and longer residence times reduce biocrude yield and increase gas and biochar formation. The pressure was found to have a minimal effect on product yield but remains essential for maintaining water in a liquid state during the process.

Our study also involved applying response surface methodology to visualize the impact of operating conditions on product yield. The model was adjusted to determine the most effective operating parameters to optimize the HTL of brown seaweeds. The results showed that the highest biocrude yield of 23% was obtained at a temperature of 283°C, pressure of 200 bar, residence time of 47 minutes, and a water-to-biomass ratio of 10:1.

Sensitivity analysis showed the critical role of the aqueous-to-biocrude reaction across all macroalgae fractions, suggesting that water-soluble compounds (WSP) are the major source of biocrude. This finding offers a significant pathway for further optimization in HTL processes.

ACKNOWLEDGMENTS

We acknowledge the Washington Sea Grant, for sponsoring this work through the grant R/SFA-10.

5.0 REFERENCES

[1] K. Anastasakis, A.B. Ross, Hydrothermal liquefaction of the brown macro-alga Laminaria Saccharina: Effect of reaction conditions on product distribution and composition, Bioresour. Technol. 102 (2011) 4876–4883. https://doi.org/10.1016/j.biortech.2011.01.031.

[2] E. Fidelis Wilson, A. Joseph Taiwo, O. Martins Chineme, A. Yusuf Temitope, E. Francis Chukwuka, A. Michael Olufemi, E. Osaretin Noah, I. Pamela Meyenum, Z. Adesanya, A Review on the Use of Natural Gas Purification Processes to Enhance Natural Gas Utilization, Int. J. Oil, Gas Coal Eng. (2023). https://doi.org/10.11648/j.ogce.20231101.13.

[3] S. Raikova, M.J. Allen, C.J. Chuck, Hydrothermal liquefaction of macroalgae for the production of renewable biofuels, Biofuels, Bioprod. Biorefining 13 (2019) 1483–1504. https://doi.org/10.1002/bbb.2047.

[4] K. Anastasakis, A.B. Ross, Hydrothermal liquefaction of four brown macro-algae commonly found on the UK coasts: An energetic analysis of the process and comparison with bio-chemical conversion methods, Fuel 139 (2015) 546–553. https://doi.org/10.1016/j.fuel.2014.09.006.

[5] P. Schiener, K.D. Black, M.S. Stanley, D.H. Green, The seasonal variation in the chemical composition of the kelp species Laminaria digitata, Laminaria hyperborea, Saccharina latissima and Alaria esculenta, J. Appl. Phycol. 27 (2015) 363–373. https://doi.org/10.1007/s10811-014-0327-1.

[6] A.M. Smith, A.B. Ross, Production of bio-coal, bio-methane and fertilizer from seaweed via hydrothermal carbonisation, Algal Res. 16 (2016) 1–11. https://doi.org/10.1016/j.algal.2016.02.026.

[7] J. Rowbotham, P. Dyer, H. Greenwell, M. Theodorou, Thermochemical processing of macroalgae: a late bloomer in the development of third-generation biofuels?, Biofuels 3 (2012) 441–461. https://doi.org/10.4155/bfs.12.29.

[8] FAO Yearbook. Fishery and Aquaculture Statistics 2019/FAO annuaire. Statistiques des pêches et

de l'aquaculture 2019/FAO anuario. Estadísticas de pesca y acuicultura 2019, FAO, 2021. https://doi.org/10.4060/cb7874t.

[9] M.G. Borines, R.L. de Leon, J.L. Cuello, Bioethanol production from the macroalgae Sargassum spp., Bioresour. Technol. 138 (2013) 22–29. https://doi.org/10.1016/j.biortech.2013.03.108.

[10] S. Wang, X.M. Jiang, N. Wang, L.J. Yu, Z. Li, P.M. He, Research on Pyrolysis Characteristics of Seaweed, Energy & Fuels 21 (2007) 3723–3729. https://doi.org/10.1021/ef700214w.

[11] S. Wang, X.M. Jiang, X.X. Han, J.G. Liu, Combustion Characteristics of Seaweed Biomass. 1. Combustion Characteristics of Enteromorpha clathrata and Sargassum natans, Energy & Fuels 23 (2009) 5173–5178. https://doi.org/10.1021/ef900414x.

[12] N. Ahmed, B.R. Dhar, B.K. Pramanik, H. Forehead, W.E. Price, F.I. Hai, A Cookbook for Bioethanol from Macroalgae: Review of Selecting and Combining Processes to Enhance Bioethanol Production, Curr. Pollut. Reports 7 (2021) 476–493. https://doi.org/10.1007/s40726-021-00202-7.

[13] P. Biller, A.B. Ross, Potential yields and properties of oil from the hydrothermal liquefaction of microalgae with different biochemical content, Bioresour. Technol. 102 (2011) 215–225. https://doi.org/10.1016/j.biortech.2010.06.028.

[14] S. Leow, J.R. Witter, D.R. Vardon, B.K. Sharma, J.S. Guest, T.J. Strathmann, Prediction of microalgae hydrothermal liquefaction products from feedstock biochemical composition, Green Chem. 17 (2015) 3584–3599. https://doi.org/10.1039/C5GC00574D.

[15] A.R.K. Gollakota, N. Kishore, S. Gu, A review on hydrothermal liquefaction of biomass, Renew. Sustain. Energy Rev. 81 (2018) 1378–1392. https://doi.org/10.1016/j.rser.2017.05.178.

[16] S.S. Toor, L. Rosendahl, A. Rudolf, Hydrothermal liquefaction of biomass: A review of subcritical water technologies, Energy 36 (2011) 2328–2342. https://doi.org/10.1016/j.energy.2011.03.013.

[17] K. Heger, M. Uematsu, E.U. Franck, The Static Dielectric Constant of Water at High Pressures and Temperatures to 500 MPa and 550°C, Berichte Der Bunsengesellschaft Für Phys. Chemie 84 (1980) 758–762. https://doi.org/10.1002/bbpc.19800840814.

[18] H.B. Rad, J.K. Sabet, F. Varaminian, STUDY OF SOLUBILITY IN SUPERCRITICAL FLUIDS: THERMODYNAMIC CONCEPTS AND MEASUREMENT METHODS - A REVIEW, Brazilian J. Chem. Eng. 36 (2019) 1367–1392. https://doi.org/10.1590/0104-6632.20190364s20170493.

[19] M. Uematsu, E.U. Franck, Static Dielectric Constant of Water and Steam, J. Phys. Chem. Ref. Data 9 (1980) 1291–1306. https://doi.org/10.1063/1.555632.

[20] R.L. Holliday, J.W. King, G.R. List, Hydrolysis of Vegetable Oils in Sub- and Supercritical Water, Ind. Eng. Chem. Res. 36 (1997) 932–935. https://doi.org/10.1021/ie960668f.

[21] J.W. King, R.L. Holliday, G.R. List, Hydrolysis of soybean oil, Green Chem. 1 (1999) 261–264. https://doi.org/10.1039/a908861j.

[22] R. Obeid, D.M. Lewis, N. Smith, T. Hall, P. van Eyk, Reaction Kinetics and Characterization of Species in Renewable Crude from Hydrothermal Liquefaction of Mixtures of Polymer Compounds To Represent Organic Fractions of Biomass Feedstocks, Energy & Fuels 34 (2020) 419–429. https://doi.org/10.1021/acs.energyfuels.9b02936.

[23] G. Teri, L. Luo, P.E. Savage, Hydrothermal Treatment of Protein, Polysaccharide, and Lipids Alone and in Mixtures, Energy & Fuels 28 (2014) 7501–7509. https://doi.org/10.1021/ef501760d.

[24] W.T. Chen, Y. Zhang, J. Zhang, G. Yu, L.C. Schideman, P. Zhang, M. Minarick, Hydrothermal liquefaction of mixed-culture algal biomass from wastewater treatment system into bio-crude oil, Bioresour. Technol. 152 (2014) 130–139. https://doi.org/10.1016/j.biortech.2013.10.111.

[25] A.-V. Galland-Irmouli, J. Fleurence, R. Lamghari, M. Luçon, C. Rouxel, O. Barbaroux, J.-P. Bronowicki, C. Villaume, J.-L. Guéant, Nutritional value of proteins from edible seaweed Palmaria palmata (dulse), J. Nutr. Biochem. 10 (1999) 353–359. https://doi.org/10.1016/S0955-2863(99)00014-5.

[26] S.M. Changi, J.L. Faeth, N. Mo, P.E. Savage, Hydrothermal Reactions of Biomolecules Relevant for Microalgae Liquefaction, Ind. Eng. Chem. Res. 54 (2015) 11733–11758. https://doi.org/10.1021/acs.iecr.5b02771.

[27] S.L. Holdt, S. Kraan, Bioactive compounds in seaweed: functional food applications and

legislation, J. Appl. Phycol. 23 (2011) 543–597. https://doi.org/10.1007/s10811-010-9632-5.

[28] M. Shameel, Phycochemicalstudiesonfattyacidsfromcertain seaweeds., BotanicaMarina (1990) 429–432.

[29] P.J. Valdez, V.J. Tocco, P.E. Savage, A general kinetic model for the hydrothermal liquefaction of microalgae, Bioresour. Technol. 163 (2014) 123–127. https://doi.org/10.1016/j.biortech.2014.04.013.

[30] C. Deng, R. Lin, X. Kang, B. Wu, X. Ning, D. Wall, J.D. Murphy, Co-production of hydrochar, levulinic acid and value-added chemicals by microwave-assisted hydrothermal carbonization of seaweed, Chem. Eng. J. 441 (2022) 135915. https://doi.org/10.1016/j.cej.2022.135915.

[31] S. Raikova, C.D. Le, T.A. Beacham, R.W. Jenkins, M.J. Allen, C.J. Chuck, Towards a marine biorefinery through the hydrothermal liquefaction of macroalgae native to the United Kingdom, Biomass and Bioenergy 107 (2017) 244–253. https://doi.org/10.1016/j.biombioe.2017.10.010.

[32] M. Déniel, G. Haarlemmer, A. Roubaud, E. Weiss-Hortala, J. Fages, Modelling and Predictive Study of Hydrothermal Liquefaction: Application to Food Processing Residues, Waste and Biomass Valorization 8 (2017) 2087–2107. https://doi.org/10.1007/s12649-016-9726-7.

[33] R. Obeid, D. Lewis, N. Smith, P. van Eyk, The elucidation of reaction kinetics for hydrothermal liquefaction of model macromolecules, Chem. Eng. J. 370 (2019) 637–645. https://doi.org/10.1016/j.cej.2019.03.240.

[34] R. Obeid, D.M. Lewis, N. Smith, T. Hall, P. van Eyk, Reaction kinetics and characterisation of species in renewable crude from hydrothermal liquefaction of monomers to represent organic fractions of biomass feedstocks, Chem. Eng. J. 389 (2020) 124397. https://doi.org/10.1016/j.cej.2020.124397.

[35] D. Zhou, L. Zhang, S. Zhang, H. Fu, J. Chen, Hydrothermal Liquefaction of Macroalgae Enteromorpha prolifera to Bio-oil, Energy & Fuels 24 (2010) 4054–4061. https://doi.org/10.1021/ef100151h.

[36] Y. Qu, X. Wei, C. Zhong, Experimental study on the direct liquefaction of Cunninghamia

lanceolata in water, Energy 28 (2003) 597–606. https://doi.org/10.1016/S0360-5442(02)00178-0.

[37] R.F. Oke Mayokun, HYDROTHERMAL LIQUEFACTION OF SACCHARINA LATISSIMA FOR THE PRODUCTION OF BIOFUEL, (2023).

[38] Q.-V.B. and K.-Q.T. and K. Q., Fast Hydrothermal Liquefaction of Macro-Alga: Characterization of Products, (2016). https://doi.org/10.3303/CET1650017.

[39] M. Černá, Seaweed Proteins and Amino Acids as Nutraceuticals, in: 2011: pp. 297–312. https://doi.org/10.1016/B978-0-12-387669-0.00024-7.

[40] D.G. Smith, E.G. Young, THE COMBINED AMINO ACIDS IN SEVERAL SPECIES OF MARINE ALGAE, J. Biol. Chem. 217 (1955) 845–853. https://doi.org/10.1016/S0021-9258(18)65949-6.

[41] J.V. Vilg, G.M. Nylund, T. Werner, L. Qvirist, J.J. Mayers, H. Pavia, I. Undeland, E. Albers, Seasonal and spatial variation in biochemical composition of Saccharina latissima during a potential harvesting season for Western Sweden, Bot. Mar. 58 (2015) 435–447. https://doi.org/10.1515/bot-2015-0034.

[42] J.R. Wagner, E.M. Mount, H.F. Giles, Design of Experiments, in: Extrusion, Elsevier, 2014: pp. 291–308. https://doi.org/10.1016/B978-1-4377-3481-2.00025-9.

[43] A.D. Chacón-Parra, P.A. Hall, D.M. Lewis, M. Glasius, P.J. van Eyk, Elucidating the Maillard Reaction Mechanism in the Hydrothermal Liquefaction of Binary Model Compound Mixtures and Spirulina, ACS Sustain. Chem. Eng. 10 (2022) 10989–11003. https://doi.org/10.1021/acssuschemeng.2c03111.

[44] R. Liu, W. Tian, S. Kong, Y. Meng, H. Wang, J. Zhang, Effects of inorganic and organic acid pretreatments on the hydrothermal liquefaction of municipal secondary sludge, Energy Convers. Manag. 174 (2018) 661–667. https://doi.org/10.1016/j.enconman.2018.08.058.

[45] J.C. Velasco Calderón, J.S. Arora, S.H. Mushrif, Mechanistic Investigation into the Formation of Humins in Acid-Catalyzed Biomass Reactions, ACS Omega 7 (2022) 44786–44795. https://doi.org/10.1021/acsomega.2c04783.

[46] A.S. Jatoi, A.A. Shah, J. Ahmed, S. Rehman, S.H. Sultan, A.K. Shah, A. Raza, N.M. Mubarak, Z. Hashmi, M.A. Usto, M. Murtaza, Hydrothermal Liquefaction of Lignocellulosic and Protein-Containing Biomass: A Comprehensive Review, Catalysts 12 (2022) 1621. https://doi.org/10.3390/catal12121621.

[47] H.. Apell, Fuels from waste, Anderson, L., Tilman, D.A., (Eds.)Academic Press. New York (1967).

[48] A. Galántai, Convergence of the Nelder-Mead method, Numer. Algorithms 90 (2022) 1043–1072. https://doi.org/10.1007/s11075-021-01221-7.

[49] D. Xu, S. Guo, L. Liu, G. Lin, Z. Wu, Y. Guo, S. Wang, Heterogeneous catalytic effects on the characteristics of water-soluble and water-insoluble biocrudes in chlorella hydrothermal liquefaction, Appl. Energy 243 (2019) 165–174. https://doi.org/10.1016/j.apenergy.2019.03.180.

[50] E.P. Resurreccion, S. Kumar, Catalytic and Non-Catalytic Hydrothermal Liquefaction of Microalgae, in: Catal. Clean Energy Environ. Sustain., Springer International Publishing, Cham, 2021: pp. 149–183. https://doi.org/10.1007/978-3-030-65017-9_6.

[51] B. Hao, D. Xu, G. Jiang, T.A. Sabri, Z. Jing, Y. Guo, Chemical reactions in the hydrothermal liquefaction of biomass and in the catalytic hydrogenation upgrading of biocrude, Green Chem. 23 (2021) 1562–1583. https://doi.org/10.1039/D0GC02893B.

[52] P. Duan, P.E. Savage, Hydrothermal Liquefaction of a Microalga with Heterogeneous Catalysts, Ind. Eng. Chem. Res. 50 (2011) 52–61. https://doi.org/10.1021/ie100758s.

[53] L. Luo, J.D. Sheehan, L. Dai, P.E. Savage, Products and Kinetics for Isothermal Hydrothermal Liquefaction of Soy Protein Concentrate, ACS Sustain. Chem. Eng. 4 (2016) 2725–2733. https://doi.org/10.1021/acssuschemeng.6b00226.

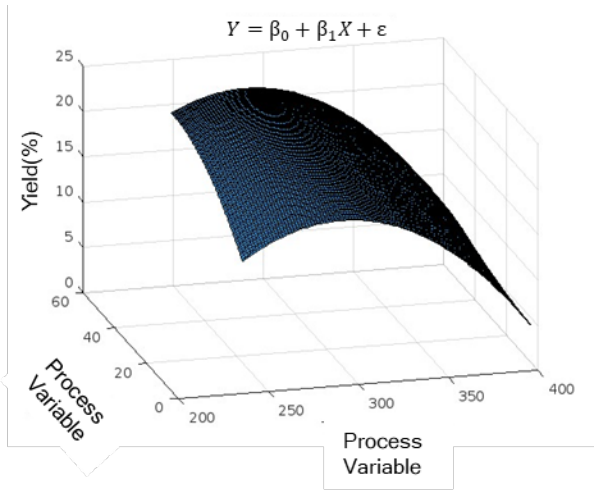

For Table of Contents Only

Supplementary Table S1

Simulation runs from design of experiment with product yields

Temperature(T)	Pressure (P)	Water/Biomass (WB)	Time (t)	Biocrude Yield(%)	Biogas Yield(%)	Biochar Yield(%)	Aqueous Product(%)
240	120	5.5000	32.5000	11.9000	6.8700	5.8300	75.4000
240	160	10	32.5000	20.1700	10.4300	7.6700	61.7300
240	200	5.5000	32.5000	11.9400	5.9000	5.8300	76.3300
400	160	1	32.5000	0.0100	28.4800	71.5100	0
320	160	5.5000	32.5000	12.8000	12.7300	6.7700	67.7000
320	200	1	32.5000	3.9700	3.5300	2.2700	90.2300
400	120	5.5000	32.5000	1.3000	71.1300	14	13.5700
240	160	1	32.5000	3.6700	1.8300	4.0300	90.4700
320	160	1	5	3	3.3000	31.6000	62.1000
320	160	1	60	3.8000	6.5700	3.9000	85.7300
320	120	1	32.5000	3.9000	4.6600	2.2700	89.1700
240	160	5.5000	60	12	10.4000	5.4000	72.2000
240	160	5.5000	5	7.4000	1.9000	46.5000	44.2000
320	120	10	32.5000	21.3600	28.2200	11.2600	39.1600
320	160	10	5	16.5300	21.2100	32.4300	29.8300
320	200	5.5000	60	12.4600	20.0100	12.6300	54.9000
400	160	10	32.5	2.2700	74.0300	23.7000	0

			000				
400	160	5.5000	60	1.5700	71.9300	26.5000	0
320	160	5.5000	32.5 000	12.8000	12.7300	6.7700	67.7000
320	160	10	60	20.7300	39.1400	21.4000	18.7300
320	120	5.5000	5	9.5700	28.8000	32.0300	29.6000
320	200	10	32.5 000	21.8300	19.2700	11.2700	47.6300
320	120	5.5000	60	12	26.3400	12.6300	49.0300
400	160	5.5000	5	1.5700	77.8600	20.5700	0
320	160	5.5000	32.5 000	12.8000	12.7300	6.7700	67.7000
320	160	5.5000	32.5 000	12.8000	12.7300	6.7700	67.7000
320	160	5.5000	32.5 000	12.8000	12.7300	6.7700	67.7000
400	200	5.5000	32.5 000	3.1000	46.4300	14	36.4700
320	200	5.5000	5	9.8300	6.9400	32.0300	51.2000

ANOVA ANALYSIS

Supplementary Table S2

Biocrude Model ANOVA Analysis

Model Terms	SumSq	DF	MeanSq	F	pValue
T	273.23	1	273.23	93.509	1.4132e-07
P	0.80083	1	0.80083	0.27408	0.6088
W_B	595.58	1	595.58	203.83	9.7661e-10
t	17.91	1	17.91	6.1294	0.026686
T:P	0.7744	1	0.7744	0.26503	0.61472
T:W_B	50.694	1	50.694	17.35	0.00095274
P:W_B	0.04	1	0.04	0.01369	0.90852
T:t	5.29	1	5.29	1.8105	0.19984
P:t	0.01	1	0.01	0.0034224	0.95418

W_B:t	2.89	1	2.89	0.98908	0.33685
T^2	216.89	1	216.89	74.229	5.7183e-07
P^2	4.6889e-28	1	4.6889e-28	1.6047e-28	1
W_B^2	0.37362	1	0.37362	0.12787	0.72599
t^2	16.347	1	16.347	5.5946	0.032987
Error	40.907	14	2.9219		

Supplementary Table S3

Gas Model ANOVA Analysis

Model Terms	SumSq	DF	MeanSq	F	pValue
T	9214.7	1	9214.7	289.56	9.4893e-11
P	340.69	1	340.69	10.706	0.0055638
W_B	1726.3	1	1726.3	54.248	3.5357e-06
t	98.499	1	98.499	3.0952	0.10035
T:P	140.78	1	140.78	4.4238	0.050004
T:WB	341.33	1	341.33	10.726	0.0055303
P:WB	15.288	1	15.288	0.48041	0.49957
T:t	52.056	1	52.056	1.6358	0.22169
P:t	60.295	1	60.295	1.8947	0.19029
W_B:t	53.729	1	53.729	1.6884	0.2148
T^2	2317.3	1	2317.3	72.82	6.4087e-07
P^2	14.888	1	14.888	0.46784	0.50515
W_B^2	23.756	1	23.756	0.74652	0.40214
t^2	345.9	1	345.9	10.87	0.0052947
Error	445.52	14	31.823		

Supplementary Table S4

Aqueous Product Model ANOVA Analysis

Model Terms	SumSq	DF	MeanSq	F	pValue
T	11426	1	11426	112.25	4.5448e-08
P	308.36	1	308.36	3.0294	0.10369
W_B	4056.1	1	4056.1	39.848	1.9147e-05
t	337.72	1	337.72	3.3178	0.089966
T:P	120.67	1	120.67	1.1855	0.29463
T:W_B	206.5	1	206.5	2.0287	0.17626
P:W_B	13.727	1	13.727	0.13486	0.71894
T:t	196	1	196	1.9255	0.18694
P:Ti	61.858	1	61.858	0.60771	0.44863
W_B:t	301.54	1	301.54	2.9624	0.10723
T^2	3033	1	3033	29.797	8.4246e-05
P^2	8.8225	1	8.8225	0.086674	0.77277
W_B^2	82.785	1	82.785	0.8133	0.3824
t^2	2155.7	1	2155.7	21.178	0.00041096
Error	1425.1	14	101.79		

Supplementary Table S5

Biochar Model ANOVA Analysis

Model Terms	SumSq	DF	MeanSq	F	pValue
T	752.4	1	752.4	4.9985	0.042173
P	8.3333e-06	1	8.3333e-06	5.5362e-08	0.99982
W_B	5.1352	1	5.1352	0.034115	0.85611
t	1058.4	1	1058.4	7.0316	0.018965
T:P	6.5955e-27	1	6.5955e-27	4.3816e-29	1
T:W_B	661.78	1	661.78	4.3964	0.054659
P:W_B	2.5e-05	1	2.5e-05	1.6608e-07	0.99968
T:t	552.96	1	552.96	3.6735	0.075926
P:t	1.7664e-27	1	1.7664e-27	1.1735e-29	1
W_B:t	69.472	1	69.472	0.46153	0.50799
T^2	469.2	1	469.2	3.1171	0.099266
P^2	46.632	1	46.632	0.30979	0.58659
W_B^2	212.69	1	212.69	1.413	0.25433
t^2	1015.9	1	1015.9	6.7493	0.021061
Error	2107.4	14	150.53		

Supplementary Table S6

Experimental data obtained from the literature[1,2,11,3–10]

Temperature (°C)	Pressure (bar)	Water/biomass	Time(minutes)	Exp. Biocrude Yield	Pred. Biocrude Yield
220	120	10	30	9.6	20.74865
240	120	10	30	11.9	21.89275
260	200	10	30	18	22.83509
280	200	10	30	19	22.54239
300	200	10	30	20.5	21.53129
320	200	10	30	18.5	19.80179
300	200	10	5	15	18.88444
300	200	10	15	18	20.25053
300	200	10	30	20.9	21.01465
300	200	10	60	18	20.81002
250	200	10	15	8.7	20.885515
275	200	10	15	15	20.25053
300	200	10	15	18	17.976405
325	200	10	15	19	14.57978
350	200	10	15	19	14.909696
370	200	10	15	15	15.01943

350	200	10	18	15.2	15.707382
350	200	10	25	16	15.65591
350	200	10	44	6	9.31166
350	200	10	60	12	15.65591
350	200	5	60	22	18.52103
350	200	10	60	23.6	21.26163
320	200	10	15	21	14.57978
330	200	10	15	23	17.38688
340	200	10	15	16.33	20.74499
350	200	10	15	14.67	19.73389
350	200	10	15	19.3	15.22558
350	200	10	15	13	14.32146
380	200	10	15	19.2	15.60222
350	200	10	15	17.6	14.57978
350	200	10	15	9.8	14.32146
350	200	10	15	17.8	14.32146
330	200	10	15	20.9	14.57978
340	200	10	15	16	14.458765
350	200	10	15	16	14.458765
360	200	10	15	19.1	14.717085
350	200	10	15	16.3	21.26163
260	180	10	15	18.14	22.45372
280	180	10	15	21.2	18.01095
300	180	10	15	18.5	18.55717

Exp. AP Yield	**Pred. AP Yield**	**Exp. Gas Yield**	**Pred. Gas Yield**	**Exp. Biochar Yield**	**Pred. Biochar Yield**
45	58.60749	25	5.65285	20	13.60764
48	62.84009	23	5.70305	17	15.98304
42	54.27917	21	6.36381	18	17.57036
40	63.33969	25	8.18841	18	18.37464
36.5	59.60669	26.5	12.38341	17	18.39084
35	43.08017	30	29.6	16.5	17.61896
37	33.57233	27	26	16	30.391575
40	42.96383	26	22.39	17	18.38874
36.5	46.93379	27	22	17	18.12138
32	30.61745	28	30.50633	25	32.886465
30	58.72344	12	8	24.5	32.25287
28	49.749785	12	12.12	18	30.393465
28	54.36944	12.8	13.14277	15	27.30384
27	45.969315	15	22.319895	12	22.985465
26	33.42044	16	33.978258	17	18.646065

24	20.39424	15	51.035754	10	20.753552
26	35.31749	14	43.67169	21	16.776565
30	38.09194	21	23.49539	17	14.666208
24	23.82587	18	43.67169	18	22.73864
26	17.27219	27.5	26.69	30	16.84499
35	47.34729	28	27.47977	26	22.73864
20	17.27219	39	40.55017	37	28.019015
25	33.42044	46	47.09217	35	26.538465
42.9	33.42044	25	34.60077	32	20.914065
27.7	33.42044	29.4	34.60077	30	18.646065
31	43.79144	34.7	34.60077	30	31.980465
30	38.93784	24	24.47977	24.5	22.985465
27	33.42044	28	29.24397	17.5	26.538465
21.5	27.23924	32	34.60077	24	24.860265
23	20.39424	35	40.55017	13.5	22.985465
39.27	51.76599	35	47.09217	14.5	20.914065
52.11	54.36944	11.67	9.48301	16.5	18.646065
46	46.09334	11.9	12.05	32.5	31.979415
27	28.35128	9.05	13.57	29.17	30.393465
26	27.506646	16	15.71497	22.5	22.987565
29	27.64319	7	6.47873	21	22.984625
30	46.62019	26	30.55069	38	21.48204
35	46.71719	21	24.64917	17	14.93784
		19	23.53965	18	22.46004

PT vs Biocrude yield

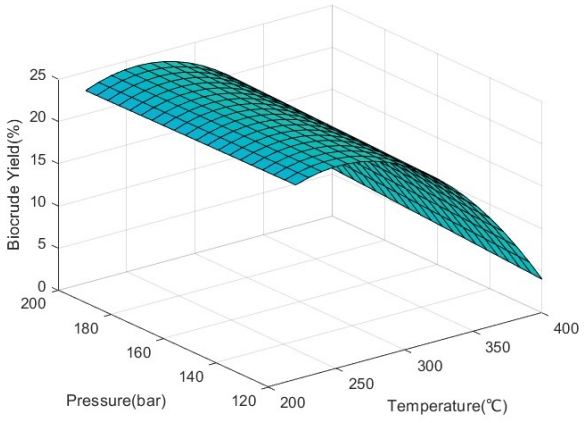

References

[1] S. Xu, L. Zou, X. Ling, Y. Wei, S. Zhang, Preparation and thermal reliability of methyl palmitate/methyl stearate mixture as a novel composite phase change material, Energy Build. 68 (2014) 372–375. https://doi.org/10.1016/j.enbuild.2013.09.038.

[2] D.C. Elliott, L.J. Sealock, R.S. Butner, Product analysis from direct liquefaction of several high-moisture biomass feedstocks, ACS Symp. Ser. (1988) 179–188. https://doi.org/10.1021/bk-1988-0376.ch017.

[3] K. Anastasakis, A.B. Ross, Hydrothermal liquefaction of the brown macro-alga Laminaria Saccharina: Effect of reaction conditions on product distribution and composition, Bioresour. Technol. 102 (2011) 4876–4883. https://doi.org/10.1016/j.biortech.2011.01.031.

[4] D. Li, L. Chen, D. Xu, X. Zhang, N. Ye, F. Chen, S. Chen, Preparation and characteristics of bio-oil from the marine brown alga Sargassum patens C. Agardh, Bioresour. Technol. 104 (2012) 737–742. https://doi.org/10.1016/j.biortech.2011.11.011.

[5] K. Anastasakis, A.B. Ross, Hydrothermal liquefaction of four brown macro-algae commonly found on the UK coasts: An energetic analysis of the process and comparison with bio-chemical conversion methods, Fuel 139 (2015) 546–553. https://doi.org/10.1016/j.fuel.2014.09.006.

[6] D. López Barreiro, M. Beck, U. Hornung, F. Ronsse, A. Kruse, W. Prins, Suitability of hydrothermal liquefaction as a conversion route to produce biofuels from macroalgae, Algal Res. 11 (2015) 234–241. https://doi.org/10.1016/j.algal.2015.06.023.

[7] S. Raikova, C.D. Le, T.A. Beacham, R.W. Jenkins, M.J. Allen, C.J. Chuck, Towards a marine biorefinery through the hydrothermal liquefaction of macroalgae native to the United Kingdom, Biomass and Bioenergy 107 (2017) 244–253. https://doi.org/10.1016/j.biombioe.2017.10.010.

[8] B. Biswas, A.C. Fernandes, J. Kumar, U.D. Muraleedharan, T. Bhaskar, Valorization of Sargassum tenerrimum: Value addition using hydrothermal liquefaction, Fuel 222 (2018) 394–401. https://doi.org/10.1016/j.fuel.2018.02.153.

[9] B. Biswas, A. Kumar, A.C. Fernandes, K. Saini, S. Negi, U.D. Muraleedharan, T. Bhaskar, Solid base catalytic hydrothermal liquefaction of macroalgae: Effects of process parameter on product yield and characterization, Bioresour. Technol. 307 (2020) 123232. https://doi.org/10.1016/j.biortech.2020.123232.

[10] D. Zhou, L. Zhang, S. Zhang, H. Fu, J. Chen, Hydrothermal Liquefaction of Macroalgae Enteromorpha prolifera to Bio-oil, Energy & Fuels 24 (2010) 4054–4061. https://doi.org/10.1021/ef100151h.

[11] M. Oke, F. Resende, Hydrothermal Liquefaction of Saccharina latissima : Effects of Catalysts, Temperature, Residence Time, and Biomass-to-Water Ratio, Energy & Fuels 37 (2023) 17345–17358. https://doi.org/10.1021/acs.energyfuels.3c02998.